Double-Stranded DNA Binding Characteristics and Subcellular Distribution of a Minor Groove Binding Diphenyl Ether Bisbenzimidazole†

Alexander L. Satz,‡ Christine M. White,§ Terry A. Beerman,*,§ and Thomas C. Bruice*,‡

Department of Chemistry and Biochemistry, University of California at Santa Barbara, Santa Barbara, California 93106, and Department of Pharmacology and Therapeutics, Roswell Park Cancer Institute, Elm and Carlton Streets, Buffalo, New York 14263

Received February 16, 2001; Revised Manuscript Received March 23, 2001

ABSTRACT: The interactions of Hoechst 33377 (H1) with 20 different oligomeric duplexes have been investigated via spectrofluorometric titrations and/or thermal denaturation experiments. H1 is shown to form 2:1 complexes with dsDNA binding sites of at least four contiguous A/T base pairs. H1 is also shown to possess the rare ability to meaningfully distinguish between different A•T rich sequences. For example, the combined equilibrium constants for complexation of the oligomeric duplex 5′-GCAATTGC-3′ (**15**) by H1 are found to be 110-fold greater than for the duplex 5′-GCTTAAGC-3′ (**16**). It is believed that the 5′-TpA-3′ dinucleotide step in **16** disrupts the rigid "A-tract" conformation of **15** and discourages minor groove binding by agents capable of recognizing longer dsDNA sequences. Molecular models are presented which elucidate the structure of the $(H1)_2$−dsDNA minor groove complex. The two H1 molecules bind to an A/T rich sequence of 6 bp in a slightly staggered, side-by-side, and antiparallel arrangement. Evidence suggests that the piperazine rings of the H1 side-by-side complex are capable of resting in the minor groove of G/C base pairs. Fluorescence microscopy studies using NIH3T3 cells indicate that H1 is capable of traversing the cytoplasmic membrane and selectively localizing to nuclear DNA. H1 also demonstrated the ability to inhibit endogenous transcription of the c-fos gene in NIH3T3 cells at micromolar concentrations. Cytotoxicity studies employing the same cell type show H1 to possess an LD_{50} of 3.5 μM.

Interest in the control of transcription at the molecular level has spurred efforts toward the development of new minor groove binding agents with greater sequence selectivity (*1*−*7*). Increased selectivity can be achieved by increasing the number of base pairs recognized by a DNA-binding agent. An alternative is to develop agents capable of distinguishing among all four DNA bases (*1*). Recently, we reported a novel tripyrrole peptide−bisbenzimidazole conjugate capable of recognizing 9 bp in the minor groove of dsDNA[1] (*8*). In a continuing effort to develop bisbenzimidazole-type compounds with increased specificity, we investigated the dsDNA binding characteristics of a diphenyl ether bisbenzimidazole H1 (*9*). H1 held the potential for recognizing dsDNA sequences longer than other bisbenzimidazole-type compounds such as H2 due to its increased length while still maintaining a crescent-shaped curvature. A crescent shape is a characteristic of bisbenzimidazoles that allows them to maintain optimal contact in the minor groove.

Although H3 is the most widely investigated of the bisbenzimidazole-type compounds, both H1 and H2 are known to be significantly more cytotoxic (*10*, *11*). It has been suggested that these agents exhibit greater cytotoxicity due to their greater cellular permeability (*11*). Minor groove binding agents can inhibit the binding of regulatory proteins to their DNA consensus sites in cell-free studies (*7*, *12*, *13*). This may be the mechanism by which H1 and H2 contribute to cell death. The cytotoxicity of H1 suggests that it possesses some type of biological activity. Previous studies did not investigate the ability of H1 to traverse the cell membrane and reach its nuclear DNA target. Quantitative determination of its ability to inhibit gene transcription in whole cells, in combination with the knowledge that it selectively localizes in nuclear DNA, would provide a much stronger link between its ability to bind DNA and its cytotoxicity.

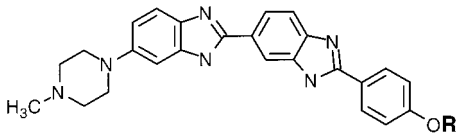

Hoechst 33377 (H1) R = -phenyl
Hoechst 33342 (H2) R = -ethyl
Hoecsht 33258 (H3) R = -H

Here we employ a combination of cell-free and cellular assays to determine if H1 would make a good lead compound for the pursuit of new minor groove binding agents with increased binding selectivity and potency. We have investigated the binding of H1 to the 18 bp oligomeric duplex 5′-GCGGTATAAAATTCGACG-3′ (**1**) and nine other related duplexes (**2**−**10**) in an effort to characterize H1's

† This work was supported by grants from the National Institutes of Health to T.C.B. (5R37DK09171-36) and the American Cancer Society to T.A.B. (RPG-96-034-04-CDD).

‡ University of California at Santa Barbara.

§ Roswell Park Cancer Institute.

[1] Abbreviations: H1, Hoechst 33377; H2, Hoechst 33342; H3, Hoechst 33258; dsDNA, double-stranded DNA; HPLC, high-pressure liquid chromatography; DMSO, dimethyl sulfoxide; Ar, aromatic; ssDNA, single-stranded DNA; TF, transcription factor; SRE, serum response element; SRF, serum response factor; EMSA, electrophoretic mobility shift assay; oligo, oligonucleotide.

10.1021/bi0103415 CCC: $20.00
Published on Web 05/04/2001

Table 1: Stoichiometries and Equilibrium Association Constants for (Ligand)$_x$−dsDNA Complexes and Relative Fluorescence Intensities[a]

oligomeric duplex[b]	H1	H2	H3
5′-GCGACTGCAATTTCGACGTCC-3′ (**11**)			
(ligand)$_x$−**11** stoichiometry	2:1	1:1	1:1
fluorescence intensity	5400	6400	6900
equilibrium association constant[d]	$K_1K_2 = 8.4 \times 10^{16}$ M^{-2}	$K_1 = 1.2 \times 10^{9}$ M^{-1}	$K_1 = 4.2 \times 10^{8}$ M^{-1}
5′-GCGACTGCAATTCGACGTCC-3′ (**12**)			
(ligand)$_x$−**12** stoichiometry	2:1	1:1	1:1
fluorescence intensity	4400	5600	6400
equilibrium association constant[d]	$K_1K_2 = 2.6 \times 10^{16}$ M^{-2}	$K_1 = 1.5 \times 10^{8}$ M^{-1}	$K_1 = 1.8 \times 10^{8}$ M^{-1}
5′-GGACGTCGATTGCAGTCGTC-3′ (**13**)			
(ligand)$_x$−**13** stoichiometry	no clear binding[c]	2:1	2:1
fluorescence intensity	140−190	4000	2500
equilibrium association constant[d]	no clear binding	$K_1K_2 = 2.3 \times 10^{14}$ M^{-2}	$K_1K_2 = 4.7 \times 10^{14}$ M^{-2}
5′-GGACGTCGTTGCAGTCGTCG-3′ (**14**)	no binding	no binding	no binding
fluorescence intensity	22	35	150
buffer only (no DNA)	22	23	160

[a] Stoichiometries determined by spectrofluorometric titration (10 mM potassium phosphate pH 7.0 buffer, 150 mM NaCl, 26 °C). Relative fluorescence intensities stated in arbitrary fluorescence units (450 nm) × M^{-1}. [b] Potential A·T rich binding sites are underlined. [c] The relative fluorescence intensity of the ligand−**13** complex is too weak to accurately measure the level of complex formation. [d] Determined by nonlinear least-squares fitting of an isothermal binding curve. Isothermal binding curves were generated using 10 mM potassium phosphate pH 7.0 buffer and 150 mM NaCl at 26 °C. Equilibrium constants are given as the product K_1K_2 for 2:1 ligand:DNA stoichiometries since separation of individual equilibrium constants is not possible. The stated equilibrium constants have a standard deviation of ±80%.

Table 2: Melting Temperatures for Ligand−18-mer Complexes (°C)[a]

18 bp oligomeric duplex	t^0_m	Δt_m H1	Δt_m H2	Δt_m H3
5′-GCGGTATAAAATTCGACG-3′ (**1**)	57	6	5	3
5′-GCGG**C**ATAAAATTCGACG-3′ (**2**)	62	4	4	2
5′-GCGG**TG**TAAAATTCGACG-3′ (**3**)	60	5	5	1
5′-GCGGTA**C**AAAATTCGACG-3′ (**4**)	60	5	5	1
5′-GCGGTAT**G**AAATTCGACG-3′ (**5**)	58	6	6	1
5′-GCGGTATA**G**AATTCGACG-3′ (**6**)	57	5	6	2
5′-GCGGTATAA**G**ATTCGACG-3′ (**7**)	57	2	2	1
5′-GCGGTATAAA**G**TTCGACG-3′ (**8**)	58	1	0	1
5′-GCGGTATAAAA**C**TCGACG-3′ (**9**)	58	3	2	1
5′-GCGGTATAAAAT**C**CGACG-3′ (**10**)	58	5	3	2

[a] t_m values for complexes were determined by first-derivative analysis. t^0_m values are melting temperatures of oligomeric duplexes (0.15 μM) in 10 mM potassium phosphate pH 7.0 buffer containing 150 mM NaCl in the absence of ligand. Δt_m values are differences in melting temperatures for oligomeric duplexes in the absence and presence (0.3 μM = 2 equiv) of ligand. The standard deviation for Δt_m values is ±1 °C.

Table 3: Melting Temperatures for Oligomeric Duplexes of the Type d(-A$_x$T$_x$-) and d(-T$_x$A$_x$-) and Their Ligand Complexes (°C)[a,b]

oligomeric duplex[c]	t^0_m	Δt_m H1	Δt_m H2	Δt_m H3	Δt_m netropsin
5′-GCAATTGC-3′ (**15**)[b]	40	12	11	8	6
5′-GCTTAAGC-3′ (**16**)[b]	30	0	11	9	4
Δt_m(**15**) − Δt_m(**16**)		12	0	−1	2
5′-GAAAATTTTC-3′ (**17**)	29	19	18	14	14
5′-GTTTTAAAAC-3′ (**18**)	24	12	16	13	12
Δt_m(**17**) − Δt_m(**18**)		7	2	1	2
5′-GAAAAAATTTTTTC-3′ (**19**)	42	15	16	13	10
5′-GTTTTTTAAAAAAC-3′ (**20**)	39	16	15	13	9
Δt_m(**19**) − Δt_m(**20**)		−1	1	0	1

[a] t_m values for oligomer complexes were determined by first-derivative analysis. All t_m values were determined by employing 1.5 μM oligomeric duplex and 3 μM ligand. t^0_m values are melting temperatures of oligomeric duplexes in the absence of ligand. Δt_m values are differences in melting temperatures for oligomeric duplexes in the absence and presence of ligand. The standard deviation for Δt_m values is ±1 °C. [b] All experiments employed 10 mM potassium phosphate pH 7.0 buffer and 150 mM NaCl except for those involving **15** and **16**, for which equivalent buffer of 1 M NaCl was used. [c] 5′-TpA-3′ dinucleotide steps are underlined.

sequence selectivity (Table 2). The oligomeric duplex **1** contains the TATA box, which in eukaryotes consists of the consensus sequence 5′-TATAAAA-3′, and is recognized by the TATA binding protein (TBP) subunit of TFIID of the RNA polymerase II transcription initiation complex. One benefit of studying bisbenzimidazoles such as H1 is that they form highly fluorescent dsDNA complexes. This makes it possible to determine dsDNA complex stoichiometries and equilibrium association constants via spectrofluorometric titrations (*8*, *14*−*16*). (H1)$_x$−dsDNA complex stoichiometries and equilibrium association constants are reported for a series of oligomeric duplexes which differ in the size of their A/T rich binding sites (Table 1). The ability of H1 to distinguish among different A/T rich oligomeric duplexes of the type d(-A$_x$T$_x$-) versus d(-T$_x$A$_x$-) (x = 2, 4, and 6) is discussed (Tables 3 and 4). Comparisons are made between H1, H2, H3, and netropsin. Additionally, we report the ability of H1 to inhibit endogenous transcription of the c-fos gene in NIH3T3 cells and describe the use of fluorescence microscopy in determining the subcellular distribution of the agent.

To determine if H1 is able to bind to nuclear DNA, the subcellular localization of H1 was explored using fluorescence microscopy. Localization to the nucleus may be connected to an agent's ability to affect DNA-related functions. Recently, H2 was demonstrated to inhibit the endogenous expression of the c-fos gene in NIH3T3 cells at micromolar concentrations (*17*). The c-fos gene, an immediate-early response gene, is tightly regulated at the level of transcription (*18*, *19*). The expression of c-fos requires a functional serum response element (SRE), a promoter region containing an A/T rich site, to which a dimer of the serum response factor (SRF) binds (*20*, *21*). This A/T rich site in the SRE is a potential target for binding by H1 and disruption of normal gene expression. Consequently, we investigate the ability of H1 to inhibit endogenous transcription of the c-fos gene in NIH3T3 cells. Finally, because the DNA binding activity of H1 may contribute to its ability to cause cell death, its cytotoxicity profile is compared to those of H2 and H3.

Table 4: Comparison of Equilibrium Association Constants for Complexation of d(GCA_2T_2GC) versus d(GCT_2A_2GC) for H1 and H3[a]

	H1	H3
5′-GCAATTGC-3′ (**15**)		
equilibrium constant	$K_1K_2 = 1.6 \times 10^{16}$ M^{-2}	$K_1 = 2.4 \times 10^{8}$ M^{-1}
$(ligand)_x$−**15** stoichiometry	2:1	1:1
fluorescence intensity ($\lambda_{max} = 450$ nm)	4260	7200
5′-GCTTAAGC-3′ (**16**)		
equilibrium constant	$K_1K_2 = 1.4 \times 10^{14}$ M^{-2}	$K_1 = 1.1 \times 10^{8}$ M^{-1}
$(ligand)_x$−**16** stoichiometry	2:1	1:1
fluorescence intensity ($\lambda_{max} = 480$ nm)	1280	500
factor change in equilibrium constant given as K_{15}/K_{16}	110	2

[a] Determined by nonlinear least-squares fitting of an isothermal binding curve. Isothermal binding curves were generated using 10 mM potassium phosphate pH 7.0 buffer and 1 M NaCl at 16.5 °C. Equilibrium constants are given as the product K_1K_2 for 2:1 ligand:DNA stoichiometries since separation of individual equilibrium constants is not possible. The stated equilibrium constants have a standard deviation of ±80%. Complex stoichiometries were determined via spectrofluorometric titrations. Fluorescence intensities are provided in arbitrary fluorescence units × M^{-1} (oligomeric duplex). Fluorescence emission was monitored at 450 or 480 nm depending on the wavelength of maximum signal intensity for the ligand−dsDNA complex (λ_{max}).

MATERIALS AND METHODS

Organic Synthesis. ^{1}H NMR spectra were obtained on a Varian Unity Inova 400 spectrometer. Fast atom bombardment mass spectra were obtained on a VG analytical, VG-70E double-focusing mass spectrometer, with an Ion Tech Xenon Gun FAB source, and an OPUS/SIOS data interface and acquisition system. High-pressure liquid chromatography was carried out using a Hewlett-Packard series 1050 HPLC system equipped with a diode array detector. For preparative separations, an Alltech Macrosphere 300A, C8, silica, 7 μm, 250 mm × 10 mm reverse phase column was used. For analytical separations, an Alltech Macrosphere 300A, C18, silica, 7 μm, 250 mm × 4.6 mm reverse phase column was used.

H1. 2-(3-Nitro-4-aminophenyl)-6-(4-methyl-1-piperazinyl)-benzimidazole (222 mg, 0.63 mmol) was hydrogenated according to literature procedure to form the reactive diortho amine 2-(3,4-diaminophenyl)-6-(4-methyl-1-piperazinyl)benzimidazole (*22*). The diortho amine was dried under vacuum for 30 min and then without purification added to 5 mL of nitrobenzene and 1 equiv of 4-phenoxybenzaldehyde (125 mg). The solution was stirred at 140 °C for 23 h. The product was precipitated out with hexanes and collected by filtration. The crude product was then purified by flash chromatography (silica, 70:30:1 ethyl acetate/methanol/triethylamine mixture). The product was then further purified via HPLC reverse phase chromatography (0.1% aqueous trifluoroacetic acid, acetonitrile mobile phase) to yield 9.25 × 10^{-6} mol of product. Quantification of product quantity was achieved via NMR spectroscopy using an internal standard. Product purity was shown by analytical HPLC analysis: $R_f = 0.1$ (silica, 70:30:1 ethyl acetate/methanol/triethylamine mixture); ^{1}H NMR (D_2O + DMSO-d_6) δ 2.85 (s, 3H, CH_3-NR_2), 3−3.1 and 3.14−3.26 [two multiplets, 4H, (-CH_2)$_2$NMe, piperazine], 3.54 and 3.84 [two doublets, 4H, -(CH_2)$_2$N-Ar, piperazine], 7.04 (m), 7.1 (m), 7.18 (m), 7.23 (m), 7.28 (m), 7.4 (m), 7.66 (m), 7.84 (m), 7.93 (m), 8.1 (m), 8.32 (m) (signals detected between 7 and 8.4 ppm are due to Ar protons); LRMS (FAB) 501 $(M + H)^+$.

DNA Binding Investigations. Purified DNA oligomers were purchased from the Biomolecular Resource Center, University of California at San Francisco (San Francisco, CA). H2, H3, 0.05 wt % 3-(trimethylsilyl)propionic-2,2,3,3-d_4 acid, sodium salt in D_2O, solvents, and other reagents were purchased from Aldrich Chemical Co. Oligomeric duplexes were formed by annealing complementary oligomers by heating equal molar mixtures to 95 °C for 10 min and slowly cooling them to ambient temperature. In the case of less thermally stable oligomeric duplexes, ssDNA oligomers were heated to 90 °C and slowly cooled to 5 °C at a rate of 2 °C/min by employing a temperature programmable cell block. Molar extinction coefficients for oligomeric duplexes were approximated using an A_{260} of 16 800 M^{-1} (G·C base pair)$^{-1}$ and an A_{260} of 13 600 M^{-1} (A·T base pair)$^{-1}$. Solutions of known ligand concentrations were prepared via peak integration of the ligand's NMR spectrum where the ligand samples that were used contained a known quantity of the internal standard 3-(trimethylsilyl)propionic-2,2,3,3-d_4 acid, sodium salt (*15*). UV−vis spectra were acquired on a Cary 100 Bio UV−vis spectrophotometer equipped with a temperature programmable cell block. Data points were taken every 1 °C with a temperature ramp of 0.5 °C/min. Thermal melting temperatures were calculated by first-derivative analysis. Fluorescence spectra were obtained on a Perkin-Elmer LS50B fluorimeter equipped with a constant-temperature water bath. Solutions were excited at 345 nm. Spectrofluorometric titrations were carried out by titrating a constant concentration of DNA, usually between 2 and 100 nM, with a relatively concentrated solution of ligand. All experiments were carried out in 10 mM potassium phosphate pH 7.0 buffer and 150 mM NaCl unless specifically stated otherwise. Buffer solutions were treated with Chelex and filtered (0.22 μm).

Following determination of ligand−dsDNA complex stoichiometries, equilibrium constants for dsDNA complexation were determined by generating isothermal binding curves via spectrofluorometric titrations (titration of a dilute dsDNA solution with ligand). Equilibrium constants for ligand−dsDNA stoichiometries were calculated by fitting isothermal binding curves using either eq 1 or 2 with eq 3 (Figure 1C) (*8*, *15*). Equations 1 and 2 were employed to fit plots of fluorescence versus concentration of unbound ligand ($[L]_f$) for cases of 1:1 and 2:1 binding stoichiometries, respectively. The $[L]_f$ is calculated using eq 3. The derivation and use of eqs 1−3 have been discussed previously (*8*, *15*, *16*).

$$F = \sum \Phi_f \left(\frac{K_1[L]_f}{1 + K_1[L]_f} \right) \quad (1)$$

$$F = \sum \Phi_f \left(\frac{0.5K_1[L]_f + K_1K_2[L]_f}{1 + K_1[L]_f + K_1K_2[L]_f} \right) \quad (2)$$

where $\sum\Phi_f$ is the total fluorescence intensity upon saturation of dsDNA binding sites with ligand while K_1 and K_2 are the equilibrium association constants for the first and second binding events, respectively.

$$F = \sum \Phi_f \frac{[L]_{bound}}{n[DNA]_T} \quad (3)$$

where $[L]_{bound}$ is the concentration of ligand bound to dsDNA, n is the stoichiometry of binding, and $[DNA]_T$ is the total concentration of duplex DNA in the sample. Equation 4 was only employed for investigation of the H3−**13** and H3−**16** complexes. It was used to calculate the fluorescence signal of the ligand−dsDNA complexes adjusted for background emission of the uncomplexed ligand (F_{adj}).

$$F_{adj} = F - [L]_f \Phi_{buffer} \quad (4)$$

where $[L]_f$ is calculated using eq 3 and Φ_{buffer} is the relative fluorescence intensity of ligand in buffer as listed in Table 1 in units of fluorescence × M^{-1}.

Model Building. The molecular modeling program SYBYL was used to construct plausible ligand−dsDNA complexes. For $(H1)_2$−dsDNA and $(H3)_2$−dsDNA complexes, ligand molecules were docked into the A/T rich minor groove of a model B-DNA helix. The 1:1 H2−, H3−, and netropsin−dsDNA complex models were derived from X-ray crystal structure coordinates (*23*, *24*). Estimates of binding site size were made by measuring the length of the bound ligand along the helix axis (angstroms) and dividing that value by 3.4 Å, the average distance that separates bases along the helix axis of B-DNA.

Cell Culture. Murine NIH3T3 fibroblasts [American Type Culture Collection (ATCC)] were passaged in Dulbecco's modified Eagle's medium (DMEM) containing high levels of glucose (4500 mg/L) and sodium pyruvate (110 mg/L), supplemented with 10% calf serum. Cells were maintained at 37 °C in 5% CO_2.

Drug Handling and Storage. H1 samples were stored as lyophilized, 10 nmol aliquots at −20 °C in a light-tight box. Samples were resuspended in dH_2O (pH 3) to a final working concentration of 1 mM and stored at −20 °C until they were used. Resuspended drug was warmed to room temperature and mixed well before further dilutions into dH_2O as noted below. H2 (Aldrich Chemical Co.) was prepared in dH_2O and treated similarly.

*Fluorescence Microscopy and Visualization of Drug Localization in Live NIH3T3 Cells***.** A total of 3.7 × 10^4 NIH3T3 cells were seeded onto 18 mm round coverslips in flat-bottomed 12-well plates and allowed to grow for 48 h. The growth medium was replaced with 0.8 mL of starvation medium (0.5% calf serum in DMEM), to which was added 10 μL of drug appropriately diluted in sterile dH_2O. After 16 h, the coverslips were pried from their wells and dip-rinsed in phosphate buffered saline. They were placed onto glass slides and observed immediately using an Olympus BX40 epifluorescence microscope equipped with a universal reflected light fluorescence vertical illuminator (Olympus, Inc.). An Olympus U-MNU filter cube was chosen to visualize the cells. Images were captured using an RT-SPOT color digital camera (Diagnostic Instruments, Inc.). Initially, the exposure time was manually set to 100 ms to accommodate the best visualization of the brightest image, and all subsequent images were captured using this exposure for any given experiment. Monochrome and color fluoromicrographs and their respective phase contrast images were captured. Duplicate coverslips for each drug exposure were evaluated in three separate experiments, and three images of different fields in each coverslip were captured to obtain representative results. Semiquantitative assessment of comparative drug intensity in the monochrome images was achieved using Diagnostic Instrument's ImagePro Plus program. The integrated optical density (IOD) of the cells was quantified and expressed per cell number in the field of view. IOD values for the three images captured per coverslip were then averaged.

Northern Blot Analysis. A total of 2.5 × 10^5 NIH3T3 cells were seeded into 60 mm plates and allowed to grow for 48 h. Following removal of growth medium and a PBS rinse, starvation medium was added. Drug dilutions were made into sterile dH_2O, and 20 μL of these dilutions was added to duplicate plates. At least three controls, which received dH_2O only, were used in each experiment. After 16 h, the cells were induced for c-fos by adding calf serum directly to the plates to a final concentration of 15% and incubating the cells at 37 °C for 30 min (previously determined to be optimal for c-fos mRNA expression). Total RNA was then isolated using TRIzol (GIBCO BRL) and electrophoresed in 1× MOPS buffer [40 mM MOPS (pH 7.0), 10 mM sodium acetate, and 10 mM EDTA] on a 1.5% denaturing agarose gel (2.2 M formaldehyde and 1× MOPS) for 4.5 h at 80 V. RNA was transferred and UV cross-linked to a GeneScreen membrane (NEN Life Science Products), incubated at 60 °C for 1 h in pre-hybe buffer [0.5 M sodium phosphate (pH 7.2), 7% SDS, 1 mM EDTA, and 1% bovine serum albumin (BSA)], and then hybridized to radiolabeled probes under the same conditions overnight. The plasmid pGEM4z-Fos (Loftstrand Laboratories, Ltd.), containing the murine c-fos coding sequence, and a phagemid containing the coding sequence for glyceraldehyde-3-phosphate dehydrogenase (G3) (ATCC) served as the probes. Each was linearized with *Hin*dIII and radiolabeled with [α-^{32}P]dCTP using Ambion's DecaPrime II kit. Blots were given two 20 min washes each in buffer A [40 mM sodium phosphate (pH 7.2), 5% SDS, 1 mM EDTA, and 0.5% BSA] and buffer B [20 mM sodium phosphate (pH 7.2), 1% SDS, and 1 mM EDTA] before being exposed to a Molecular Dynamics phosphorimaging screen and scanned with the company's STORM phosphorimager. Quantitation using the company's ImageQuant program allowed percent growth inhibition to be calculated by comparing drug-treated samples to solvent controls.

Cytotoxicity Assay. A total of 1 × 10^4 NIH3T3 cells were seeded into each well of a 24-well plate and allowed to grow for 24 h. Growth medium was removed and replaced with 0.4 mL of fresh growth medium. Drug was diluted into sterile dH_2O, and 10 μL of appropriate dilutions was added to each well. Triplicate samples for each drug concentration per experiment were carried out. In total, three experiments were performed. Cells were allowed to grow for 72 h before being trypsinized and counted using a automated particle counter (Beckman Coulter, Inc.). Percent cell survival was calculated by comparing drug-treated samples to solvent controls.

RESULTS

Synthesis of H1. H1 was originally synthesized via two consecutive reactions of diortho amines with imino ethers

to form the molecule's two benzimidazole rings (*9*). Our slightly modified approach took advantage of a reaction pioneered by Lown and co-workers that involves condensation of a diortho amine with an aldehyde in nitrobenzene solvent to give the final product (*25*). The ^{1}H NMR data for H1, previously unreported, are included in Materials and Methods.

*Spectrofluorometric Titrations of Oligomeric Duplexes **11**−**14** (15).* Similar to that of H3 (*14*, *15*), the fluorescence emission intensities of H1 and H2 greatly increase upon complexation with dsDNA. When excited at 345 nm, H1− and H2−dsDNA complexes emit a broad fluorescence signal centered at 450 nm. Table 1 lists stoichiometries of (ligand)$_x$−dsDNA complexes and their relative fluorescence intensities at 450 nm.

H1 forms 2:1 ligand−dsDNA complexes with oligomeric duplexes **11** and **12**. H2 and H3 form complexes with the same oligomers with 1:1 stoichiometries. The fluorescence spectra of H1 and H2 in pH 7.0 buffer (no DNA present) consist of a featureless straight line between 410 and 490 nm. In contrast, the uncomplexed fluorescence spectrum of H3 has a broad plateau or peak which begins to increase at ∼460 nm and reaches a maximum at wavelengths of ≥480 nm.

The fluorescence spectrum of H1 in the presence of **13** contains a broad peak centered at 450 nm, characteristic of an (H1)$_x$−dsDNA complex. However, the instability and weak fluorescence of the (H1)$_x$−**13** complex prevented its stoichiometry from being determined accurately. H2− and H3−**13** complexes were found to have 2:1 stoichiometries. Titration of **13** with 1 equiv of H3 effects a pronounced peak centered at 450 nm within the fluorescence spectrum, which is characteristic of H3−dsDNA complexes. Later in the titration, at points with >1 equiv of H3, the solution's fluorescence spectrum shifts to the red and begins to resemble that expected for uncomplexed H3. As shown in Figure 1A, the high background fluorescence of uncomplexed H3 obscures the fluorescence emission of the (H3)$_2$−**13** complex. The later part of the titration (Figure 1A) describes a straight line with a slope of 1.76×10^8 M^{-1}, roughly equivalent to the value of 1.6×10^8 M^{-1} determined for uncomplexed H3 in pH 7.0 buffer. The magnitude of the fluorescence signal due to uncomplexed H3 was subtracted from each data point (eq 4) to yield a plot of $F_{adjusted}$ versus [H3]$_0$ from which the stoichiometry of the complex was determined (Figure 1B). Additionally, an isothermal binding curve was plotted and the equilibrium constant for complexation of **13** calculated (Figure 1C). Relative fluorescence intensities for ligands in the presence of oligomeric duplex **14** are equivalent to those observed in buffer only (Table 1).

*Equilibrium Association Constants for Complexation of Oligomeric Duplexes **11**−**13**.* All three ligands formed complexes with **11** and **12** at near-nanomolar concentrations (Table 1). Comparison between equilibrium constants determined in units of M^{-2} and M^{-1} can be made by calculating the square root of K_1K_2 values to give approximate equilibrium constants for individual binding events in units of M^{-1}. By this approximation, the equilibrium constant for complexation of **12** by H1 (K_1) is $\sim 1.6 \times 10^8$ M^{-1}, equivalent to the K_1 values for H2 and H3. Using this same method, K_1 values for complexation of **13** by H2 and H3 are $\sim 1.5 \times 10^7$ and 2.2×10^7 M^{-1}, respectively. Hence, binding of H2 and H3 to the oligomeric duplex **13** yields a K_1 value that is 10-fold lower than that obtained with duplex **12**.

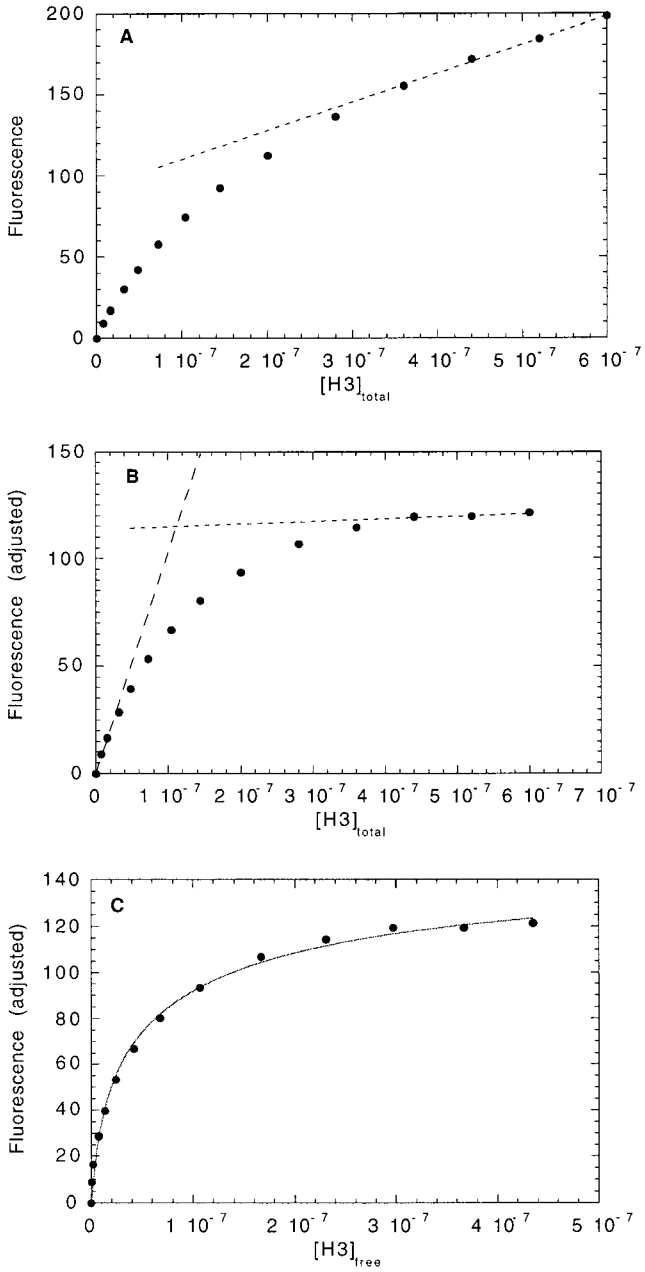

FIGURE 1: (A) Titration of 50 nM **13** with H3. The plot shows the relative fluorescence intensity at 450 nm in arbitrary units vs [H3]$_{total}$. The straight line was generated by linear least-squares fitting of data points late in the titration ($y = 92.51 + 1.77 \times 10^8$). (B) The fluorescence data from panel A have been adjusted to account for fluorescence due to uncomplexed (free) H3 using eq 4. The straight lines were generated by linear least-squares fitting of data points early and late in the titration. The two lines intersect at 100 nM, indicating formation of an (H3)$_2$−**13** complex. (C) The fluorescence data from panel B have been plotted vs [H3]$_{free}$ as calculated by eq 3. The data have been fit by a nonlinear least-squares fitting routine by employing eq 2 to determine the equilibrium association constant for complexation (for the fit shown in panel C, $R^2 = 0.99$).

The effects of ligands on the thermal stabilities of oligomeric duplexes **11**−**14** were investigated in an attempt to compare the effects with values ascertained via spectrofluorometric titrations. However, ligands had little effect on the thermal stabilities of **11**−**14** even when employing low-

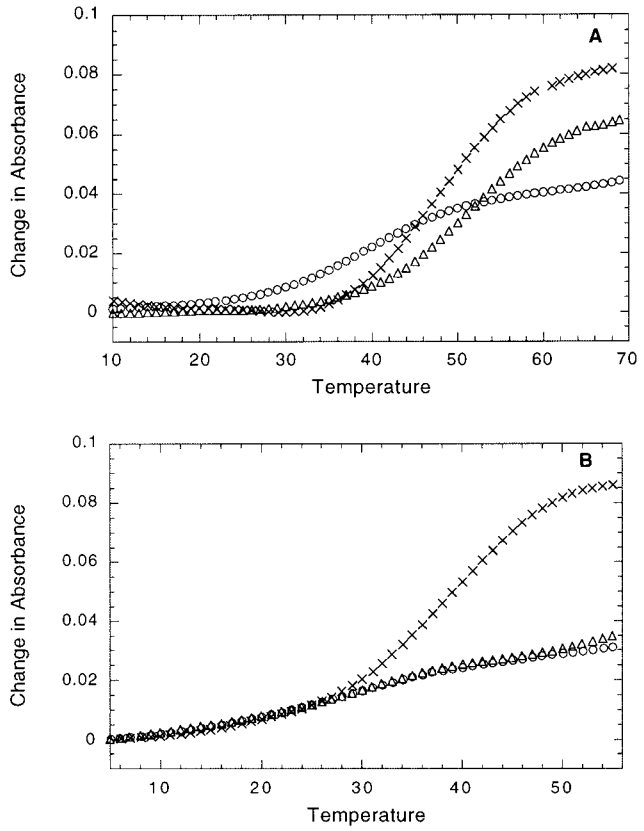

FIGURE 2: Thermal melting curves for oligomeric duplexes **15** (A) and **16** (B) and their ligand (2 equiv) complexes. Plots are shown as the change in absorption units vs degrees Celsius. Experiments were carried out using 1.5 μM duplex and 3 μM ligand, 10 mM potassium phosphate pH 7.0 buffer, and 1 M NaCl: DNA with H1 (△), DNA with H3 (×), and DNA with no ligand (○).

salt buffer (10 mM NaCl) due to intrinsically large t^0_m values (otherwise, thermal melting experiments employing **11**−**14** were carried out under the conditions provided in Table 2). H1−H3 each raised the melting point of **11** from 59 to 64 °C. Ligand Δt_m values were 1 °C or less for oligomeric duplexes **12**−**14**.

Thermal Stability of Ligand−18-mer Complexes. The thermal stabilities of (ligand)$_x$−dsDNA complexes for H1 are little affected by base pair changes of the type A/T → G/C within the TATAA region of **1** (Table 2). In contrast, H1 is very sensitive to A/T → G/C base pair changes in several other positions within **1** as illustrated by the small Δt_m values for oligomeric duplexes **7**−**9**. Thus, the increased thermal stability of the (H1)$_x$−**1** complex is attributed to complex formation between H1 and the duplex's AAATT region. Binding of **1**'s TATAA region by H1 appears to be so weak that A·T → G·C mutations have little effect on the overall thermal stability of the complexes. The Δt_m values for H2 show a similar trend to those for H1. Overall, The Δt_m values for H3 are too small to assess the ligand's sequence selectivity.

*Thermal Stability of Oligomeric Duplexes **15**−**20** and Their Ligand Complexes*. Thermal melting temperatures for a series of oligomeric duplexes are listed in Table 3 (Figure 2). Each pair contains an oligomeric duplex lacking a 5′-TpA-3′ step (**15**, **17**, and **19**) and a duplex containing a 5′-TpA-3′ dinucleotide in the middle of its A/T rich binding site (**16**, **18**, and **20**). H1 shows a tremendous preference for **15** over **16** and a significant preference for **17** over **18**. The (H1)$_2$−**15** complex has a Δt_m of 12 °C, and its melting curve shows a large increase in the hyperchromicity of the duplex. In contrast, the (H1)$_2$−**16** complex has a Δt_m of 0 °C and its melting curve shows no enhancement of the hyperchromicity of the duplex (Figure 2B). The Δt_m values for H1 complexes of **19** and **20** are equivalent. As shown in Table 3, neither H2, H3, nor netropsin demonstrates the selectively exhibited by H1.

*Equilibrium Constants for Complexation of **15** and **16** by H1 and H3.* As for oligomeric duplexes **11** and **12**, H1 formed 2:1 complexes with both **15** and **16** while H3 formed 1:1 complexes (Table 4). The K_1K_2 value for complexation of **15** by H1 was found to be 110-fold greater than for **16**. The fluorescence emission of the H3−**16** complex was found to be relatively weak. As was seen for the H3−**13** complex, the fluorescence signal of uncomplexed H3 obscured that of the H3−dsDNA complex such that it had to be subtracted out by employing eq 4. Fluorescence spectra for both H1 and H3 complexes with **16** displayed a peak with its maxima centered at ∼480 nm, red-shifted approximately 30 nm compared to spectra of "normal" ligand−DNA complexes such as those for **11** and **12**. Spectrofluorometric titrations were conducted under conditions of high salt (1 M NaCl) and low temperature (16.5 °C) to stabilize the short oligomeric duplex **16**.

Estimation of Binding Site Size via Model Building. A plausible structure of a side-by-side (H1)$_2$−dsDNA complex was constructed, and its binding site size was measured to be 6.2 bp (Figures 3 and 4). With the piperazine rings not being counted, the side-by-side dimer was estimated to extend 14 Å along the helix axis and cover 4.1 bp. Binding site sizes for several other types of ligand−dsDNA complexes were also estimated (Figure 4).

Localization of H1 in Cells. To determine if H1 is able to enter nuclei, NIH3T3 cells were plated onto coverslips and exposed to the agent for 16 h in starvation medium (DMEM with 0.5% calf serum). Starvation conditions were chosen so that appropriate comparisons could be made to subsequent Northern blot experiments, which require starving NIH3T3 cells overnight in preparation for evaluation of drug effects on c-fos gene expression. Since H1 is a Hoechst analogue, cells were exposed to H2 under the same conditions to compare localization of the two compounds. The cells were not fixed or mounted following exposure to drug. Rather, the coverslips were simply transferred to glass slides and viewed immediately, when the cells were still alive. Representative fluoromicrographs (Figure 5A′,B′) of cells exposed to 1 μM H1 or 0.5 μM H2 show that both compounds localize exclusively to nuclei with similar staining patterns. While diffuse nuclear staining is observed, small regions of high drug concentrations exist as evidenced by areas of high fluorescence intensity. This speckled pattern for either drug does not always correspond to nucleoli, visible in the corresponding phase contrast micrographs. Overall, treatment of cells with 0.5 μM H2 yields nuclei that are slightly brighter than those treated with 1 μM H1. The staining on any given coverslip was fairly even, with little variation between viewing fields. These and additional images captured using a range of drug concentrations as well as semiquantitative analysis of the resulting fluoromicrographs (data not shown) demonstrated that approximately 4 times more H1 was

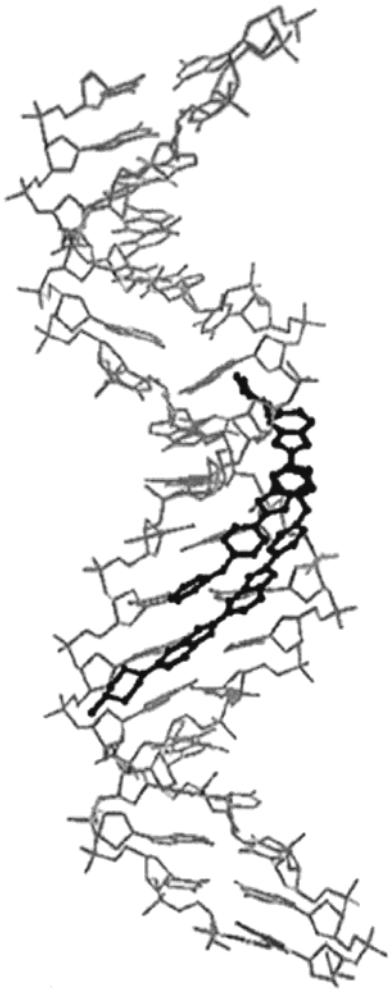

FIGURE 3: Computer-generated model of a plausible $(H1)_2$−dsDNA side-by-side antiparallel staggered complex.

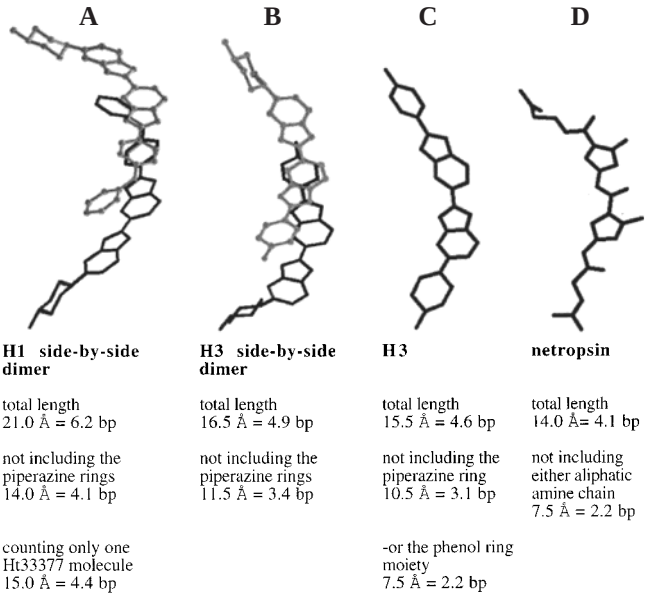

FIGURE 4: Ligands were extracted from computer-generated $(ligand)_x$−dsDNA models and are pictured in their dsDNA-bound conformations (DNA atoms are not shown so that ligand curvature can be better displayed). Estimated binding site sizes of $(ligand)_x$−dsDNA complexes are provided below the pictured ligands. Also generated but not pictured was the 1:1 H2−dsDNA complex whose binding site size was estimated to be 17.5 Å (5.1 bp).

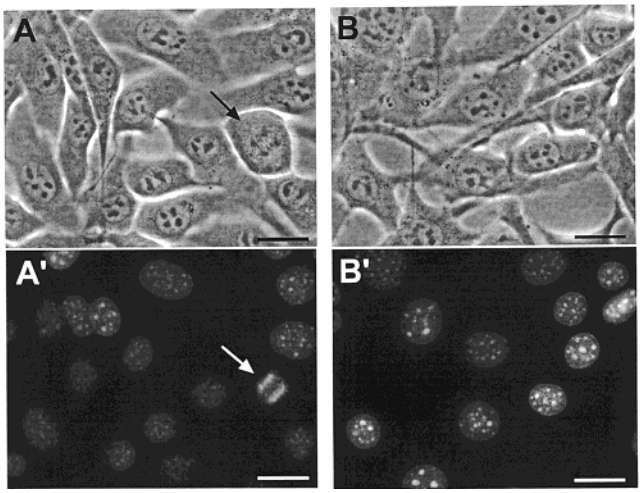

FIGURE 5: Localization of H2 and H1 to nuclei in live NIH3T3 cells. (A and A′) Representative phase contrast and fluoromicrographs, respectively, of NIH3T3 cells exposed to 1 μM H1 for 16 h. (B and B′) Representative phase contrast and fluoromicrographs, respectively, of NIH3T3 cells exposed to 0.5 μM H2 for 16 h. Images were captured immediately following transfer of coverslips of live cells to glass slides. H1 localizes to nuclear material, even in actively dividing cells (arrows). The bars are 10 μm in length.

required to attain the same level of H2 fluorescence intensity. A cell captured in the process of mitosis (Figure 5A,A′, arrows) shows that H1 associates with nuclear material even during division.

Effects of H1 on Endogenous c-fos mRNA Expression. The presence of H1 in the nucleus suggested that it may have DNA template effects in whole cells. The c-fos promoter has been established in the Beerman lab as a model system for evaluating the effect of DNA-binding drugs on transcription (*17*). Therefore, H1's effects on endogenous transcription of the c-fos gene in whole cells were evaluated. NIH3T3 cells were exposed to H1 for 16 h under starvation conditions before being serum induced for 30 min, which was previously determined to be an optimal time course for c-fos mRNA production. Control cells upregulate c-fos in response to serum stimulation, as detected in Northern blots (Figure 6A, first two lanes). Glyceraldehyde-3-phosphate dehydrogenase (G3), a constitutively expressed housekeeping gene, was used here as a loading control. The half-lives of G3 and c-fos mRNA are 8 h and 30 min, respectively. Therefore, drug effects on the total amount of G3 mRNA are expected to be minimal after only 16 h. Treatment of cells with H1 led to a dose-dependent inhibition of c-fos transcription, as evidenced by the loss in signal intensity (Figure 6A, lanes 3−6). There was no detectable drug effect on G3 expression, nor was there detection of shorter transcripts for either c-fos or G3. Quantitation of the Northern blot autoradiographs allowed drug-treated samples to be compared to controls, yielding a measurement of percent inhibition of c-fos expression (Figure 6B). A maximum concentration of 10 μM H1 was used, resulting in approximately 70% inhibition of expression. Inhibition of expression by 50% (the IC_{50} value) occurred at approximately 4 μM. To note, H2 had very little effect on c-fos expression at this time point, although inhibition was seen for shorter exposures of 1 and 4 h (*17*). In contrast, H1 had no effect on c-fos expression after these shorter exposures (data not shown).

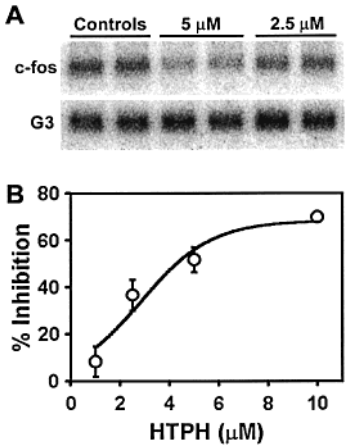

FIGURE 6: Effect of H1 on c-fos mRNA expression. (A) Representative Northern blot results from NIH3T3 cells exposed to H1 at the concentrations shown for 16 h under starvation conditions (0.5% serum). Following induction of c-fos by increasing the serum concentration to 15% for 30 min, 20 μg of total RNA was isolated and electrophoresed on a denaturing agarose gel. Subsequent blots were hybridized with radiolabeled probes for c-fos or G3. (B) Quantitation of H1's effects on c-fos cellular transcription was achieved through densitometric analysis of blots as shown in panel A. Comparison of drug-treated lanes to controls yielded percent inhibition for each treatment. The results are the means of four experiments (mean ± standard error).

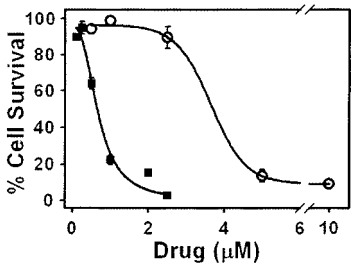

FIGURE 7: Cytotoxicity of H1 in NIH3T3 cells. Cells were allowed to grow in the presence of either H1 (○) or H2 (■) for 3 days before being trypsinized and counted. Percent cell survival was calculated by comparing the total cell number in drug-treated samples to solvent controls. The results are the means of triplicate samples in three separate experiments (mean ± standard error).

Cytotoxic Effects of H1. NIH3T3 cells were continuously exposed to a range of H1 or H2 concentrations for 3 days before being trypsinized and counted. Total cell numbers from each treatment were compared to appropriate solvent controls to yield percent cell survival. As shown in Figure 7, the concentration of H1 needed to kill 50% of the cells (LD_{50}) was 3.4 μM. By 10 μM H1, more than 90% cell death was observed. In comparison, the LD_{50} of H2 was 0.6 μM, and more than 95% of the cells died by 2.5 μM. Treatment of cells with 100 μM H3 over the same time period effected approximately 50% cell death.

DISCUSSION

Spectrofluorometric titrations were employed in an effort to determine the dsDNA binding characteristics of H1 (Table 1). H1 is shown to form $(H1)_2$−dsDNA complexes and to require a minimum binding site of 4 A/T bp. In contrast, H2 and H3 will form complexes with 3 A/T bp, although both ligands do prefer larger sites. The requirement of only 3 A/T bp for strong binding is an interesting observation since it is commonly reported that these agents require at least 4 A/T bp (*1*, *26*). Additionally, the $(H3)_2$−**13** complex stoichiometry of 2:1 is rather uncommon since such a stoichiometry has been previously reported only once for H3 (*16*). The difference in binding stoichiometries between H1 and H3 for normal size binding sites (4−5 bp) is not unexpected. It has been previously noted by this laboratory that changes in the terminal phenyl ring of H3 can alter the stoichiometries of its dsDNA complexes (*15*). The possibility that ligand−dsDNA stoichiometries determined via spectrofluorometric titrations might be misleading due to alternative modes of ligand binding has also been considered. H3 is know to interact with dsDNA by a secondary form of binding [probably intercalation (*27*)] which occurs at relatively high ligand:base pair ratios, shows no apparent base pair specificity, and is weakened considerably with increasing ionic strength (*28*). Relative fluorescence intensities for ligands in buffer with and without **14** were compared to determine if secondary forms of binding could be affecting our fluorescence measurements. The relative fluorescence intensities of H1−H3 were found to be unaffected by the addition of **14**. Thus, either no secondary form of dsDNA binding occurs at the concentrations of dsDNA that are employed, or they occur but are not detected by fluorescence spectroscopy. Either way, secondary forms of binding by H3 can only affect the observed stoichiometries if they occur in competition with H3's primary form of dsDNA binding (minor groove binding of A/T rich sites). This is unlikely since H3's secondary form of binding is roughly 100−1000-fold weaker than its primary form (*28*, *29*). Additionally, our observed stoichiometries (Table 1) are inconsistent with a competitive but nonspecific secondary form of binding.

A plausible $(H1)_2$−dsDNA complex constructed via model building illustrates the curvature of the two H1 molecules when placed in a slightly staggered, side-by-side, and antiparallel arrangement within the minor groove (Figure 3). This type of side-by-side arrangement within the minor groove has precedence since monocationic minor groove binders such as distamycin-based compounds have a propensity to complex dsDNA in this manner (*2*, *30*−*32*). When the molecules are staggered, the placement of the phenoxy ether ring of one H1 molecule adjacent to the bulky piperazine ring of the other is avoided. Structural investigations of side-by-side complexes of other minor groove binders such as polyamides with dsDNA consistently show the two polyamide molecules of the trimeric complex to be both antiparallel and staggered (*2*, *30*−*32*).

Inspection of the $(H1)_2$−dsDNA model suggests a binding site size of 6.2 bp versus an experimentally determined minimum binding site of 4 A/T bp (Figure 4). The 2 bp difference is interpreted as a lack of binding specificity on the part of H1's piperazine rings. Some X-ray crystal structures of H3−dsDNA complexes show the bisbenzimidazole rings of H3 bound to an A/T rich binding site while the piperazine ring rests against an adjacent G·C base pair (*24*, *33*). When the piperazine rings are excluded, the H1 side-by-side complex covers 4.1 bp, in agreement with the experimentally determined minimum A·T rich binding site size.

If the piperazine rings of $(H1)_2$−dsDNA complexes are capable of resting in the wider minor groove of G/C base pairs, it stands to reason that the piperizine rings of H2 and H3 might also. The binding site size of an $(H3)_2$−dsDNA

side-by-side complex was estimated to be 4.9 bp versus an experimentally determined minimum binding site size of 3 A/T bp. When the piperazine rings are excluded, the H3 side-by-side complex covers ~3.4 bp, roughly equivalent to the experimentally determined minimum A/T rich binding site size. The side-by-side $(H3)_2$−dsDNA complex was constructed in a manner similar to that of the $(H1)_2$−dsDNA complex with the two H1 molecules placed in a slightly staggered, side-by-side, and antiparallel arrangement within the minor groove.

As shown in Table 2, H1 selectively stabilizes those oligomeric duplexes which contain 4 bp A/T rich binding sites free of a 5′-TpA-3′ dinucleotide step (i.e., 4 bp "A-tracts"). A similar trend was observed for H2. It has been suggested that the 5′-TpA-3′ step produces a DNA structural alteration which discourages minor groove binding (*23*, *34*). Dickerson and co-workers have reported that A/T rich regions of dsDNA usually adopt poly(dA)/poly(dT)-like structures (termed A-tracts) (*35*, *36*). A-tracts consist of successive adenine bases which stack in a rigid and unbent column. Dickerson and co-workers emphasize that the A-tract structure can incorporate 5′-ApT-3′ steps, but is broken by 5′-TpA-3′ steps.

It was previously reported that the terbenzimidazole 5PTB was capable of selectively stabilizing **17** relative to **18** (*37*). The duplex **17** (5′-GA_4T_4C-3′) contains an uninterrupted 8 bp A tract, assumes a rigid A-tract conformation, and exhibits an anomalously slow migration in a polyacrylamide gel (*38*). The other duplex, **18** (5′-GT_4A_4C-3′), contains two 4 bp A tracts separated by a TpA dinucleotide, assumes a normal "B-like" conformation, and, on the basis of its molecular weight, migrates normally. The duplexes have also been shown to possess differential thermodynamic properties (**17** possesses a larger t^0_m than **18**) (*37*). These complexes have identical base compositions, yet evidence suggests that **17** is conformationally distinct from **18**. It was argued that the origin of 5PTB's selectivity was an entropically driven preference for highly solvated A-tracts such as those found within **17** (*37*). We have found that H1 also selectively stabilizes **17** relative to **18** (Table 3). We have also employed two additional pairs of oligomeric duplexes differing in the lengths of their A·T tracts: the pair **15** (5′-GCA_2T_2GC-3′) and **16** (5′-GCT_2A_2GC-3′), and the pair **19** (5′-GA_6T_6C-3′) and **20** (5′-GT_6A_6C-3′). Both previously uncharacterized pairs of duplexes exhibit differential thermodynamic properties similar to those of **17** and **18**. As shown by the values listed in Table 3, those duplexes containing a 5′-TpA-3′ dinucleotide have lower t^0_m values than those without. The $\Delta\Delta t_m$ values listed in Table 4 are unimpressive for all the ligands investigated except for H1 which selectively stabilizes **15** and **17** over **16** and **18** with $\Delta\Delta t_m$ values of 12 and 7 °C, respectively. The equilibrium constants for complexation of **15** with H1 were determined to be 110-fold larger than those for **16** (Table 4).

The selectivities of the different ligands can be explained in terms of the number of bases covered by their sequence selective moieties. As discussed earlier, the piperazine rings of the H1 side-by-side dimer are incapable of differentiating between A/T and G/C base pairs. Presumably, they are also incapable of selecting against 5′-TpA-3′ steps. When the piperazine rings are excluded, the H1 side-by-side dimer is estimated to have a sequence selective binding region which covers about 4.2 bp and prefers A-tracts over A/T rich sites containing 5′-TpA-3′ steps. H1 does not selectively stabilize **19** over **20** since H1 side-by-side complex formation may occur with an A-tract on either side of the dinucleotide 5′-TpA-3′ located within the middle of **20**. When the piperazine ring is not included, H2 is estimated to cover roughly 3.7 bp. The lack of selectivity of H2 for **17** over **18** can perhaps be explained in that the ligand can bind an A-tract on either side of the dinucleotide 5′-TpA-3′ located in the middle of **18**. However, this same rationale fails to explain H2's lack of selectivity between the shorter duplexes **15** and **16** unless the sequence selective moieties of H2 cover significantly less than 3.7 bp. The phenolic group of H3 has been shown by NMR spectroscopic investigations to rapidly rotate (at a rate of $>10^3$ s^{-1}) while the molecule is still bound within the minor groove (*39*, *40*). We propose that the phenol ring of H1 may not significantly contribute to the ligand's sequence selectivity. Alone, the bisbenzimidazole rings of H2 and H3 cover roughly 2.2 bp. Thus, H2 may complex **16** with its bisbenzimidazole rings on one side or the other of the 5′-TpA-3′ step. Netropsin's lack of selectivity between duplexes **15** and **16** can also be rationalized in terms of the size of its sequence selective binding site. When the agent's highly flexible aliphatic moieties are not included, netropsin is also estimated to recognize roughly 2.2 bp.

The subcellular distribution of H1 was investigated in an effort to determine if H1 was capable of associating with DNA in live cells (Figure 5). Visualization of H1 by fluorescence microscopy shows that this compound selectively localizes in the nucleus. H1 is therefore capable of traversing both the cytoplasmic and nuclear membranes and accumulating in the nucleus in a pattern suggestive of DNA binding. As previously mentioned, DNA binding agents such as H1 have the potential to act as template poisons by preventing the binding of various nuclear proteins to their DNA target sites (*7*, *41*). However, the ability of a ligand to bind DNA in vitro does not ensure its cellular activity. We demonstrate here that H1 inhibits endogenous transcription of the c-fos gene in whole cells at micromolar concentrations (Figure 6). These results suggest that H1 possesses the ability to reach its cellular target and is capable of inhibiting the binding of regulatory proteins. Our finding that H1 causes cell death at micromolar concentrations demonstrates that it is capable of disrupting normal cell function. The results of our cellular investigations for H1 and H2 were fairly similar. H3 showed little cellular activity in accord with literature reports (*10*, *11*). Apparently, alkylation of the terminal phenoxy moiety of H3 imparts upon both these molecules a superior ability to traverse the cell membrane and reach its DNA target.

CONCLUSIONS

The formation of a side-by-side complex with dsDNA appears to impart upon H1 a rare degree of sequence specificity. This may be due to the aromatic rings of the H1 side-by-side complex being held more rigidly in comparison to a 1:1 complex as for H2 or H3. Only two other types of minor groove binding agents are capable of distinguishing between different A/T rich sequences, and of the three, the mechanism by which H1 achieves its specificity is unique. The previously mentioned terbenzimidazole 5PTB forms only 1:1 complexes with **15** and **16** (*37*). Dervan and co-workers

have investigated a series of heteropolyamide hairpin-type molecules which contain various combinations of pyrrole, imidazole, and hydroxypyrrole subunits (*42*, *43*). These types of heteropolyamide molecules have, in some cases, demonstrated the ability to distinguish between A·T and T·A base pairs. However, the mechanism of heteropolyamide specificity is intrinsically different from that for H1 since heteropolyamide specificity is not related to the presence of A-tracts (heteropolyamides target sites which contain both A/T and G/C base pairs).

Evaluation of H1's biological potential revealed that it possesses many characteristics that are desirable for a DNA-reactive drug, including cellular permeability and nuclear localization, and an ability to decrease the level of gene expression. We believe that the unique mechanism of H1's specificity, combined with its ability to localize in nuclear DNA and inhibit RNA transcription, makes it a valuable starting point for the development of other sequence selective agents.

REFERENCES

1. Reddy, B. S. P., Sondhi, S. M., and Lown, J. W. (1999) *Pharmacol. Ther. 84*, 1−111.
2. Sharma, S. K., Tandon, M., and Lown, J. W. (2000) *J. Org. Chem. 65*, 1102−1107.
3. Xuereb, H., Maletic, M., Gildersleeve, J., Pelczer, I., and Kahne, D. (2000) *J. Am. Chem. Soc. 122*, 1883−1890.
4. Zimmer, C., and Wähnert, U. (1986) *Prog. Biophys. Mol. Biol. 47*, 31−112.
5. Boger, D. L., and Johnson, D. S. (1996) *Angew. Chem., Int. Ed. 35*, 1438−1474.
6. Bailly, C., and Chaires, J. B. (1998) *Bioconjugate Chem. 9*, 513−538.
7. Chiang, S. Y., Bruice, T. C., Azizkhan, J. C., Gawron, L., and Beerman, T. A. (1997) *Proc. Natl. Acad. Sci. U.S.A. 94*, 2811−2816.
8. Satz, A. L., and Bruice, T. C. (2001) *J. Am. Chem. Soc. 123*, 2469−2477.
9. Loewe, V. H., and Urbanietz, J. (1974) *Arzneim.-Forsch. 24*, 1927−1933.
10. Harapanhalli, R. S., Howell, R. W., and Rao, D. V. (1994) *Nucl. Med. Biol. 21*, 641−647.
11. Finlay, G. J., and Baguley, B. C. (1990) *Eur. J. Cancer 26*, 586−589.
12. Bruice, T. C., Sengupta, D., Blasko, A., Chiang, S. Y., and Beerman, T. A. (1997) *Bioorg. Med. Chem. 5*, 685−692.
13. Dorn, A., Affolter, M., Muller, M., Gehring, W. J., and Leupin, W. (1992) *EMBO J. 11*, 279−286.
14. Loontiens, F. G., Regenfuss, P., Zechel, A., Dumortier, L., and Clegg, R. M. (1990) *Biochemistry 29*, 9029−9039.
15. Satz, A. L., and Bruice, T. C. (2000) *Bioorg. Med. Chem. 8*, 1871−1880.
16. Browne, K. A., He, G. X., and Bruice, T. C. (1993) *J. Am. Chem. Soc. 115*, 7072−7079.
17. White, C. M., Heidenreich, O., Nordheim, A., and Beerman, T. A. (2000) *Biochemistry 39*, 12262−12273.
18. Nigg, E. A., and Treisman, R. (1994) *Curr. Opin. Cell Biol. 6*, 333−334.
19. Inada, K., Okada, S., Phuchareon, J., Hatano, M., Sugimoto, T., Moriya, H., and Tokuhisa, T. (1998) *J. Immunol. 161*, 3853−3861.
20. Treisman, R. (1985) *Cell 42*, 889−902.
21. Norman, C., Runswick, M., Pollock, R., and Treisman, R. (1988) *Cell 55*, 989−1003.
22. Ebrahimi, S. E. S., Bibby, M. C., Fox, K. R., and Douglas, K. T. (1995) *Anti-Cancer Drug Des. 10*, 463−479.
23. Ward, B., Rehfuss, R., Goodisman, J., and Dabrowiak, J. C. (1988) *Biochemistry 27*, 1198−1205.
24. Carrondo, M., Coll, M., Aymami, J., Wang, A. H. J., Vandermarel, G. A., Vanboom, J. H., and Rich, A. (1989) *Biochemistry 28*, 7849−7859.
25. Yadagiri, B., and Lown, J. W. (1990) *Synth. Commun. 20*, 955−963.
26. Harshman, K. D., and Dervan, P. B. (1985) *Nucleic Acids Res. 13*, 4825.
27. Moon, J. H., Kim, S. K., Sehlstedt, U., Rodger, A., and Norden, B. (1996) *Biopolymers 38*, 593−606.
28. Jorgenson, K. F., Varshney, U., and van de Sande, J. H. (1988) *J. Biomol. Struct. Dyn. 5*, 1005−1023.
29. Rao, K. E., and Lown, J. W. (1991) *Chem. Res. Toxicol. 4*, 661−669.
30. Kopka, M. L., Goodsell, D. S., Han, G. W., Chiu, T. K., Lown, J. W., and Dickerson, R. E. (1997) *Structure 5*, 1033−1046.
31. Wemmer, D. (1998) *Nat. Struct. Biol. 5*, 169−171.
32. Kielkopf, C. L., Baird, E. E., Dervan, P. B., and Rees, D. C. (1998) *Nat. Struct. Biol. 5*, 104−109.
33. Pjura, P. E., Grzeskowiak, K., and Dickerson, R. E. (1987) *J. Mol. Biol. 197*, 257−271.
34. Chen, F. M., and Sha, F. (1998) *Biochemistry 37*, 11143−11151.
35. Goodsell, D. S., Kaczorgrzeskowiak, M., and Dickerson, R. E. (1994) *J. Mol. Biol. 239*, 79−96.
36. Dickerson, R. E., Goodsell, D., and Kopka, M. L. (1996) *J. Mol. Biol. 256*, 108−125.
37. Pilch, D. S., Xu, Z. T., Sun, Q., LaVoie, E. J., Liu, L. F., and Breslauer, K. J. (1997) *Proc. Natl. Acad. Sci. U.S.A. 94*, 13565−13570.
38. Chen, J.-H., Seeman, N. C., and Kallenbach, N. R. (1988) *Nucleic Acids Res. 16*, 6803−6815.
39. BostockSmith, G. E., Laughton, C. A., and Searle, M. S. (1998) *Nucleic Acids Res. 26*, 1660−1667.
40. Embrey, K. J., Searle, M. S., and Craik, D. J. (1993) *Eur. J. Biochem. 211*, 437−447.
41. Mote, J., Ghanouni, P., and Reines, D. (1994) *J. Mol. Biol. 236*, 725−737.
42. Urbach, A. R., Szewczyk, J. W., White, S., Turner, J. M., Baird, E. E., and Dervan, P. B. (1999) *J. Am. Chem. Soc. 121*, 11621−11629.
43. Melander, C., Herman, D. M., and Dervan, P. B. (2000) *Chem. Eur. J. 6*, 4487−4497.

BI0103415